



Electrochemical properties of tin oxide anodes for sodium-ion batteries



Ying Ching Lu^a, Chuze Ma^c, Judith Alvarado^c, Takafumi Kidera^a, Nikolay Dimov^b, Ying Shirley Meng^c, Shigeto Okada^{b,*}

^a Department of Chemical Engineering, Faculty of Engineering, Kyushu University, Fukuoka 816-8580, Japan

^b Institute for Materials Chemistry and Engineering, Kyushu University, Fukuoka 816-8580, Japan

^c Department of NanoEngineering, University of California San Diego, La Jolla, CA 92037, USA

H I G H L I G H T S

- SnO showed the best anode performances among the Sn oxide anodes.
- Nyquist plots proved that conductivity of SnO/C anode is larger than SnO₂/C.
- Conversion reaction in SnO and SnO₂/C were confirmed by ex-situ XRD.
- After the initial cycle, SnO and SnO₂/C showed similar structure in SAED.

A R T I C L E I N F O

Article history:

Received 17 November 2014

Received in revised form

3 March 2015

Accepted 6 March 2015

Available online 6 March 2015

Keywords:

Sodium-ion battery

Tin oxide anode

Hydrothermal

SnO

SnO₂

A B S T R A C T

Few tin (Sn)-oxide based anode materials have been found to have large reversible capacity for both sodium (Na)-ion and lithium (Li)-ion batteries. Herein, we report the synthesis and electrochemical properties of Sn oxide-based anodes for sodium-ion batteries: SnO, SnO₂, and SnO₂/C. Among them, SnO is the most suitable anode for Na-ion batteries with less first cycle irreversibility, better cycle life, and lower charge transfer resistance. The energy storage mechanism of the above-mentioned Sn oxides was studied, which suggested that the conversion reaction of the Sn oxide anodes is reversible in Na-ion batteries. The better anode performance of SnO is attributed by the better conductivity.

© 2015 Elsevier B.V. All rights reserved.

1. Introduction

Because of their high energy density, lithium-ion batteries (LIB) have attracted a great deal of attention for large-scale applications beyond their traditional use in portable electronics. However, high material cost hinders the wide commercialization for large-scale applications. Therefore, sodium-ion batteries (SIB) are being considered as possible minor metal-free drop-down replacements for their lithium-ion (Li-ion) counterparts.

Despite the resemblance between Li-ion and Na-ion chemistries, there are substantial differences. It appears that there are many more cathode candidates for SIBs than for LIBs [1–4]. On the

other hand, the anode choices are severely restricted due to the sodium's unique characteristics, which hinder intercalation into the layered graphite structure in normal electrolytes [5]. Even with the diglyme based electrolyte, capacity is limited to 100 mAh/g [6]. Therefore, state-of-the-art highly crystalline graphite anodes for LIB are not suitable anodes for SIB. In addition, Li-ion alloys electrochemically with several elements that could be potentially employed as anodes; however, Na-ion does so with fewer elements [7]. It is known that silicon (Si) readily alloys with Li-ion but does not react with Na-ion at potentials down to 0 V vs. Na/Na⁺, thus Si is electrochemically inactive with Na at room temperature [7]. For that reason, most of the research of the Na alloys were focused on the Sn, P, and Sb. A. Darwiche compared the electrochemical properties of bulk Sb in the Na and Li, bulk Sb demonstrated the Na storage close to 600 mAh/g over 160 cycle with 99% coulombic efficiency [8]. J. Qian reported that Sb/C nanocomposite anode

* Corresponding author.

E-mail address: s-okada@cm.kyushu-u.ac.jp (S. Okada).

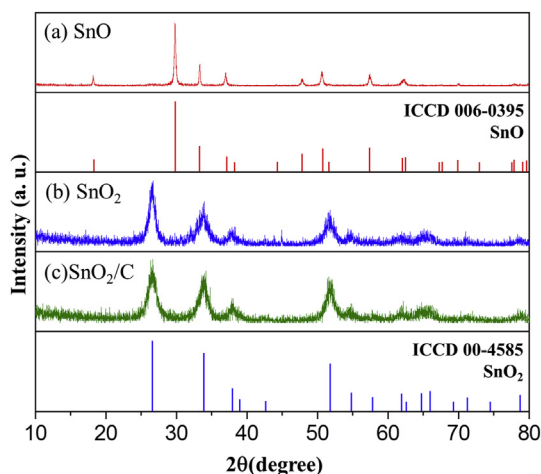


Fig. 1. XRD patterns of: (a) SnO, (b) SnO₂, and (c) SnO₂/C. SnO shows the highest crystallinity, indicated by the sharp SnO reflections. SnO₂ and SnO₂/C show diffuse and broad peaks.

delivers a capacity of 610 mAh/g at 100 mA/g and have high capacity retention over 100 cycles against Na [9]. L. Wu reported Sb–C nanofibers with large reversible capacity (631 mAh/g) at C/15 (40 mA/g) and the good rate capability [10]. J. Qian and Y. Kim showed an amorphous red phosphorus/carbon composite and it delivers 1764 mAh/g at the current density of 250 mA/g and 1890 mAh/g at current density of 143 mA/g, respectively [11,12]. Sn is also one of the few elements that can readily alloy not only with Li, but also with Na [13,14]. However, the poor cycling performance owing to the large volume expansion and unstable solid electrolyte interface (SEI) morphology are major drawbacks [15]. On the other hand, Sn oxides can be reduced by conversion with Na, this generates Sn which further alloys with Na [16–20]. It is expected that Na₂O which forms during conversion reaction, can prevent agglomeration and reduce the volume expansion of Sn. Therefore, Sn oxide could potentially be used as an anode material for Na-ion storage. M. Shimizu reported that SnO thin film anode for SIB delivers 250 mAh/g at 50 mA/g for over 50 cycles [16]. Wang's group

demonstrated that hierarchical mesoporous SnO microspheres anode for SIB exhibits reversible capacity of ca. 580 mAh/g at 20 mA/g with long cycle life [17]. Wang's group also showed that the electrochemical performance of SnO₂ [18], SnO₂@MWCNT [19], and SnO₂@graphene [20] outperformed the hard carbon anode in SIB. However, only few have discussed the reaction mechanism and the suitability of various Sn oxide anodes for SIB [17,18]. The purpose of this investigation is to compare the electrochemical performance of Sn(II) and Sn(IV) oxides as anode materials for SIBs. Both SnO and SnO₂ samples were prepared and examined by means of ex-situ XRD, TEM, SAED, and impedance spectroscopy.

2. Experimental

Both SnO and SnO₂/C anode materials were prepared by slightly modified hydrothermal methods. SnCl₂·2H₂O and SnCl₄·5H₂O were used as precursors to synthesize SnO and SnO₂, respectively.

SnO was prepared by the following typical synthetic route. First, 1 g SnCl₂·H₂O (Sigma–Aldrich, 98% purity) was dissolved in 50 ml 0.25 M citric acid (Wako). The citric acid was used as an antioxidant to prevent the oxidation of SnO to SnO₂. Then, approximately 20% aqueous ammonia solution was added drop wise to adjust the solution to pH 10 and promote the precipitation of SnO. The solution was then poured into a Teflon-sealed autoclave and heated at 150 °C for 12 h. After filtration, pure SnO precipitates were washed with distilled water and ethanol (EtOH) three times to remove contaminants and dried at 80 °C overnight. We could not get SnO/C composite because SnO was oxidized to SnO₂ during the decomposition of carbon precursor.

SnO₂/C composite was prepared in a similar manner. First, 1 g SnCl₄·5H₂O (Wako, 98% purity) was dissolved in 0.2 M glucose solution and ~20 wt% ammonia solution was added drop-wise until pH 10 was reached. The solution was then poured into a Teflon-sealed autoclave and heated at 180 °C for 12 h. At this temperature, glucose was partly carbonized and coated the SnO₂ particles. The precipitate was further washed and dried similar to the SnO sample. The sample was finally treated at 550 °C for 3 h under Ar. A reference carbon-free SnO₂ sample was also prepared by dissolving 1 g SnCl₄·5H₂O in 50 ml deionized water and treated similar to

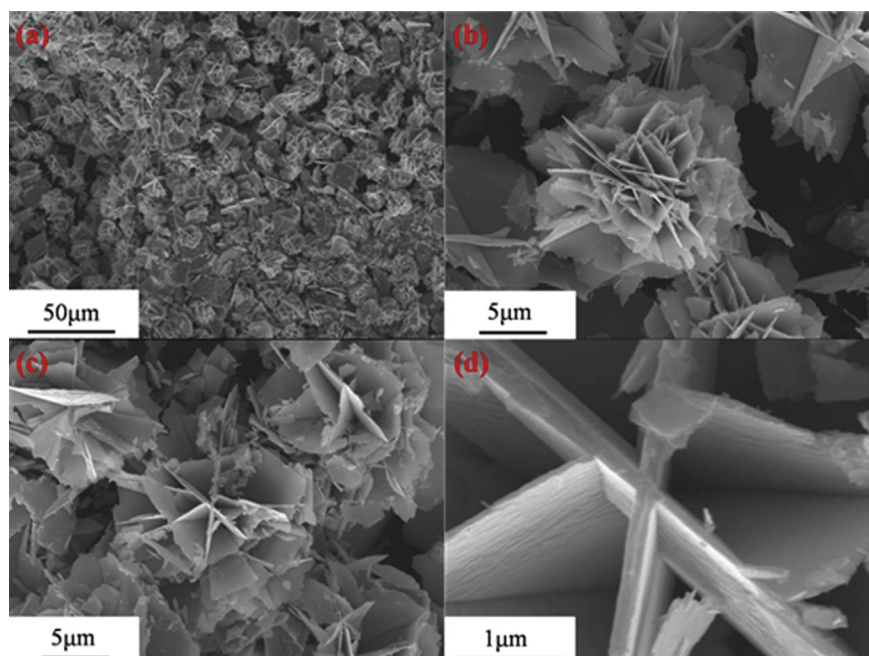


Fig. 2. SEM images: (a) Low magnification image of SnO; (b), (c) medium magnification images of flower-like SnO; (d) layer-shape grains of SnO.

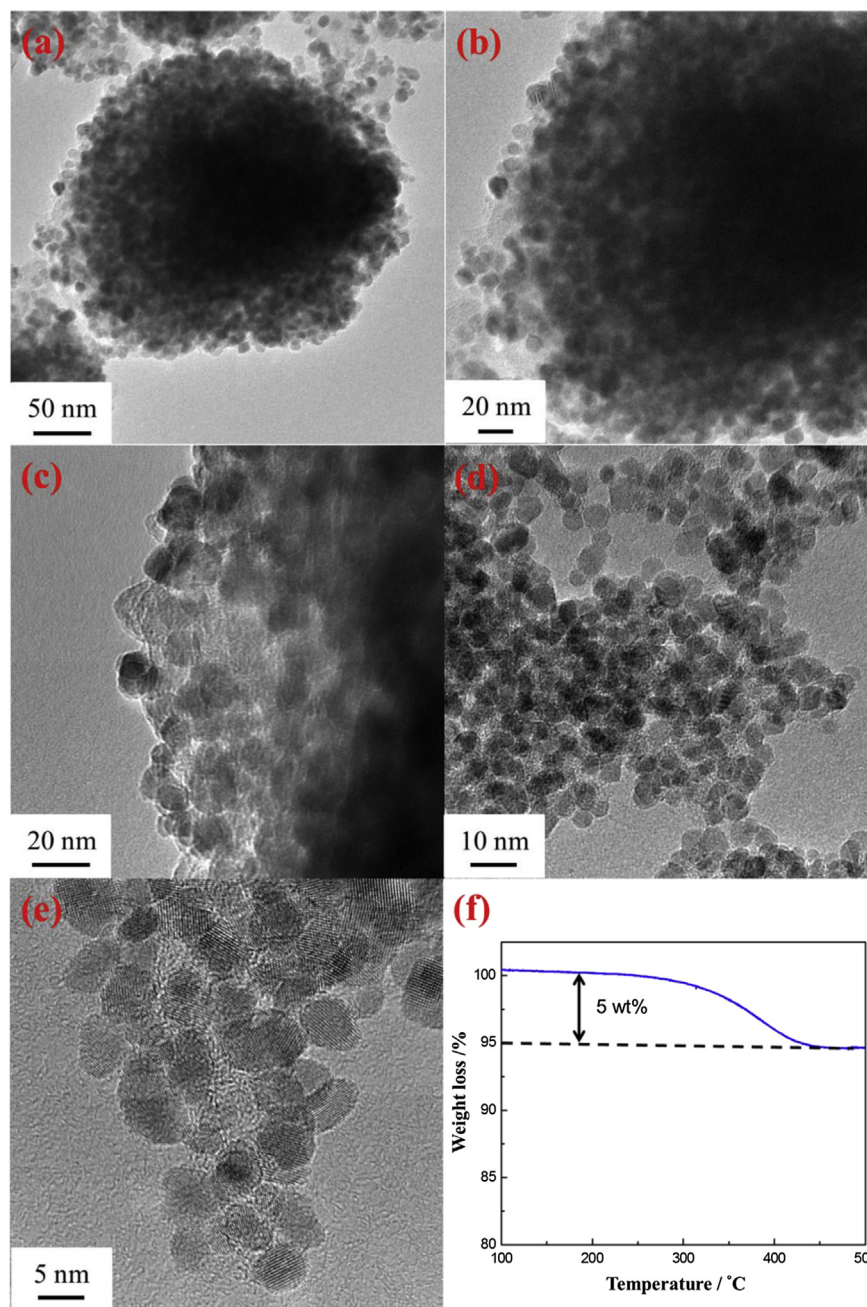


Fig. 3. TEM images: (a), (b), SnO_2 ; (c), (d), (e) TEM images of SnO_2/C ; (f) TG curve of the SnO_2/C sample heated in the air at $5\text{ }^\circ\text{C min}^{-1}$.

SnO_2/C . In the absence of glucose, pure SnO_2 phase was obtained and used for comparison with the SnO_2/C material. Phase purity and crystallinity of the samples were determined by X-ray diffraction with high intensity Cu-K α radiation (XRD, Rigaku RINT 2100, Japan). Particle size and particle morphology were observed by transmission electron microscopy (TEM, JEM2100F, JEOL, Japan). Carbon content in the SnO_2/C composite was measured by TG-DSC (Rigaku, Thermo Plus TG8210). The electrode after discharge and charge were collected using an FEI Tecnai G2 Sphera cryoelectron microscope with an operation voltage of 200 kV. The TEM and SAED images were recorded by a Gatan Ultrascan 1000 UHS CCD camera.

Electrochemical measurements were carried out in two electrode 2032 coin cells (Hohsen, Japan). Electrodes were prepared by mixing appropriate amounts of the SnO_x/AB mixture with 2 wt%

aqueous solution of carboxymethyl cellulose (CMC, MW = 700,000, Aldrich). The ingredients were put in a polypropylene vial with 3 g zirconia balls (3 mm ϕ). The vials were then placed in a rocking mill (Seiwa Giken, Japan) and were mixed for 60 min at 50 Hz to form slurry. The slurry was then coated using the doctor blade technique on a 20 μm Cu foil current collector and dried under vacuum at 80 $^\circ\text{C}$. The electrode sheets were roll-pressed, and $\phi 15$ mm electrodes were punched. The electrode composition was 70 wt% SnO_x -active material, 20 wt% AB, and 10 wt% CMC. Sodium metal foil was used as a counter electrode, and the electrolyte was 1 M NaPF_6 dissolved in ethylene carbonate (EC) and dimethyl carbonate (DMC) 1:1 by volume (Toyama Chemicals, Japan). Cycle life and rate performance testing were performed under different current densities in the voltage range of 5 mV–2.0 V.

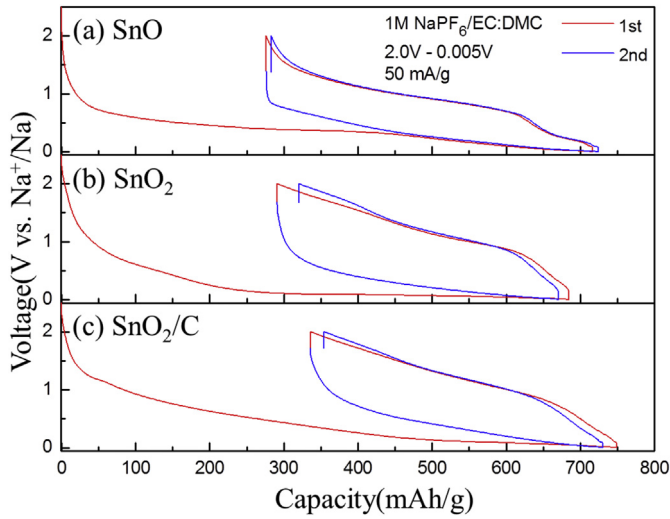


Fig. 4. Charge/discharge profiles of (a) SnO, (b) SnO₂, and (c) SnO₂/C.

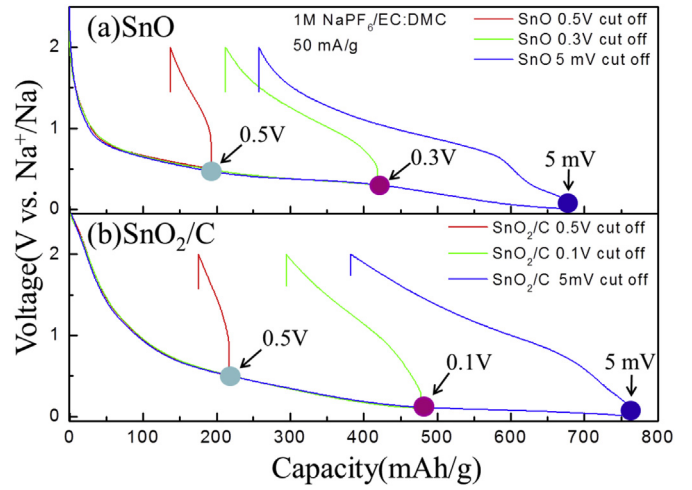


Fig. 6. Charge/discharge profiles of SnO (a) and SnO₂/C (b) at various cutoff voltages.

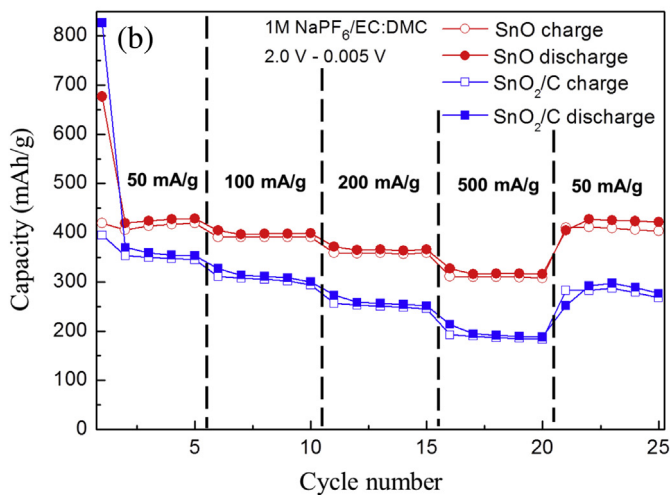
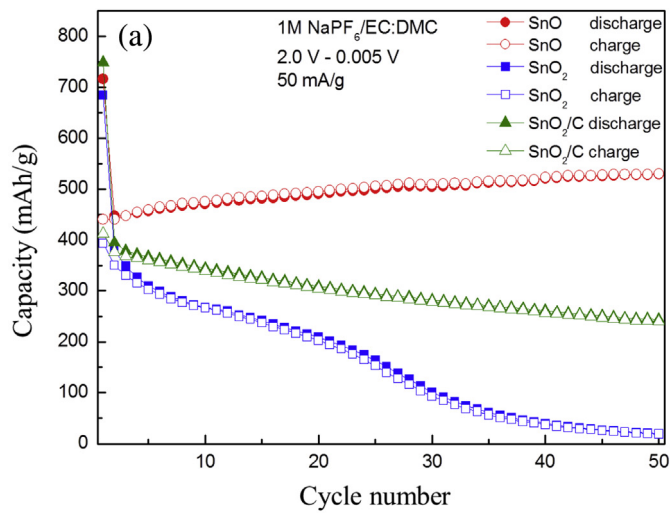


Fig. 5. (a) Cycle life of SnO, SnO₂, and SnO₂/C electrodes; (b) Rate capabilities of the SnO and SnO₂/C electrodes.

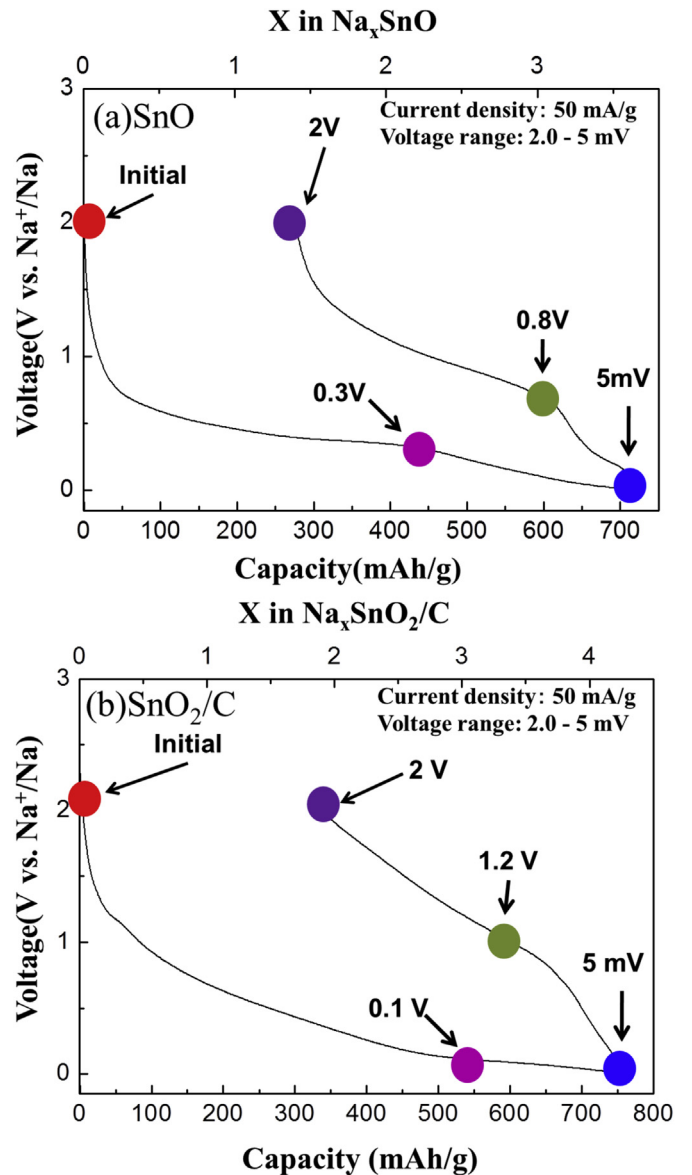


Fig. 7. Sampling points for *ex-situ* XRD (a) SnO (b) SnO₂/C.

3. Results and discussion

Fig. 1 shows the XRD patterns of the as-prepared SnO, SnO₂, and SnO₂/C samples. The results indicate that the samples are pure phase without any impurities. The morphology of SnO was observed by SEM as shown in Fig. 2. SnO particles have a flower-like morphology with a particle size distribution ranging from 5 to 10 μm. Each flower-like SnO consists of layer-shaped grains with an approximate thickness of 200 nm. This result is in consistent with the data reported by Pires et al. [21] and Macías et al. [22].

Conversely, all SnO₂-related reflections in both SnO₂ and SnO₂/C samples are very broad and the estimated particle size by the Scherrer equation yields 5–10 nm, which is in accordance with the TEM data (Fig. 3). A comparison of SnO₂ and SnO₂/C samples in Fig. 3 shows that the carbon phase formed by the hydrothermal treatment not only reduces the particle size, but also prevents particle agglomeration during the synthesis. It clearly shows that there is clustering and agglomeration of the SnO₂ nanoparticles without glucose, while the SnO₂/C particles in Fig. 3(c–e) are

separated due to the carbon coating. The TG: DSC data shown in Fig. 3(f) indicates a weight ratio of 95:5 for SnO₂:C.

Fig. 4 shows the voltage profiles of the first two cycles for SnO, SnO₂, and SnO₂/C anodes at a current density of 50 mA g⁻¹. The reversible capacities of the first cycle are 440, 393, and 412 mAh g⁻¹ with coulombic efficiencies of 61.5%, 58.5%, and 55.3%, respectively.

Fig. 5(a) compares the cycling performance of the SnO, SnO₂, and SnO₂/C samples. Pure SnO₂ demonstrates inferior capacity retention that only 4.5% of the initial capacity is maintained after 50 cycles. The SnO₂ nanocrystals coated with C (SnO₂/C) shows improved cycle life, with 58% capacity retention over 50 cycles. Not only does SnO show the best cycling performance, but the reversible capacity gradually increases over prolonged cycles. After 50 cycles, the reversible capacity of the SnO electrode increased to 530 mAh g⁻¹, a 20% increase from the second cycle. More details are discussed for this phenomenon in the later part.

The SnO electrode also exhibits superior rate capability. It delivers 440 mAh g⁻¹ at 50 mA g⁻¹ and 311 mAh g⁻¹ even at a high current density of 500 mA g⁻¹. In contrast, SnO₂/C delivers

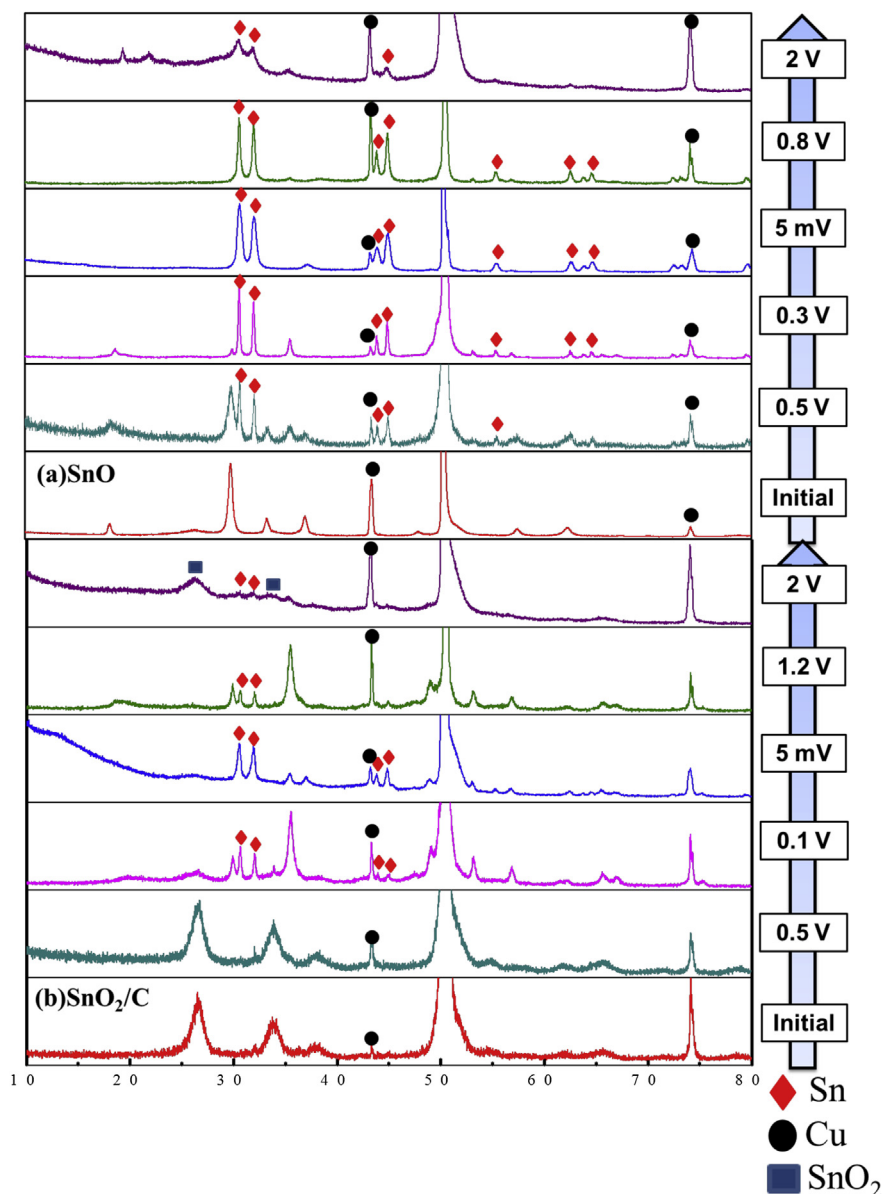


Fig. 8. Ex-situ XRD profiles of (a) SnO and (b) SnO₂/C electrodes over the first charge/discharge cycle.

411 mAh g⁻¹ at 50 mA g⁻¹ and only 192 mAh g⁻¹ at 500 mA g⁻¹. The reversible capacity of the pure SnO₂ is close to zero at 500 mA g⁻¹ (not shown in the graph).

The discharge/charge voltage profiles of the first cycle of SnO and SnO₂/C at various cutoff voltages are shown in Fig. 6. At discharge states of 0.3 V, the SnO electrode yields a specific capacity of 419 mAh/g, with a coulombic efficiency of 49.4% after charged to 2.0 V. While for the SnO₂/C electrode, it is discharged to 0.1 V, and then charged back to 2.0 V. It has a higher capacity of 478 mAh/g during the discharge; however, it yields a lower coulombic efficiency of 38.5%. Further decreasing the cutoff voltage to 5 mV increases the coulombic efficiencies to 61.7% and 52.5% for SnO and SnO₂/C, respectively. It is noteworthy that the poor coulombic efficiencies is improved by having a lower cutoff voltage. The low

coulombic efficiencies at narrow cycle depth down to 0.5 V can be attributed to the irreversible consumption of Na⁺ during the decomposition of electrolyte to form the SEI.

To gain deeper insight into these reactions, the structural transformation of the electrochemically active SnO and SnO₂/C electrodes were investigated by *ex-situ* XRD at different states of charge during the first sodiation/desodiation cycle as shown in Fig. 7. Fig. 8(a) and (b) show the XRD patterns of SnO and SnO₂/C over the first discharge/charge cycle. Strong Sn-related diffraction patterns are found in the 0.3 V SnO and 0.1 V SnO₂/C samples. The fully discharged (down to 5 mV vs. Na/Na⁺) samples show complete conversion of SnO and SnO₂/C. Even at this point, all Sn-related diffraction peaks were still strong. The presence of Sn peaks outshining the other phases (Na_xSn) even at 5 mV means that

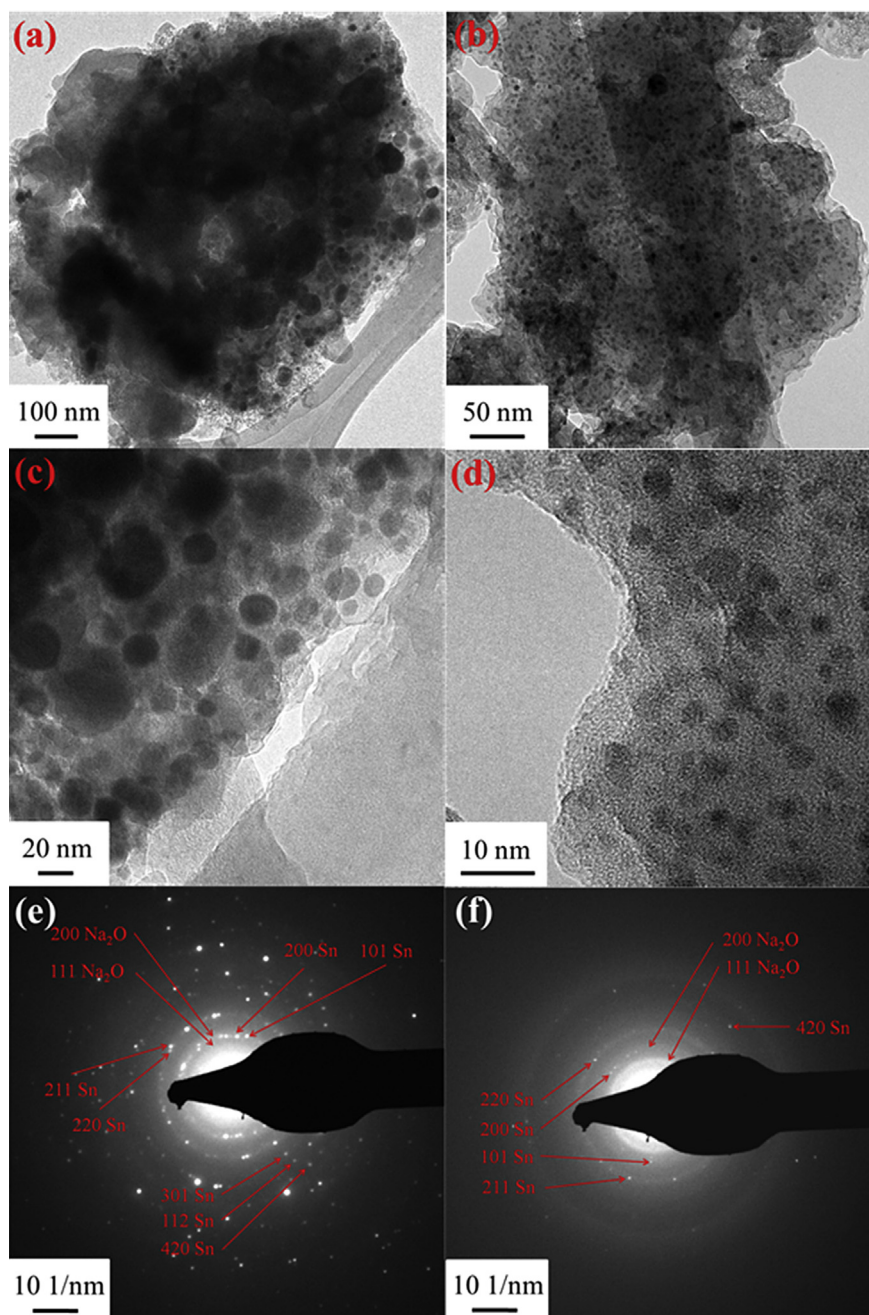


Fig. 9. TEM images: (a), (c) SnO; (b), (d) SnO₂/C after discharged to 5 mV; (e) SAED pattern of SnO discharged to 5 mV; (f) SAED pattern of SnO₂/C discharged to 5 mV.

complete sodiation of either SnO or SnO₂/C could not be achieved under our experimental conditions (50 mA g⁻¹). Charging (Na⁺ extraction) of both electrodes resulted in the gradual disappearance of the Sn-related diffractions. TEM images of the SnO and SnO₂/C electrodes at fully discharged states are shown in Fig. 9. The initial discharge of both SnO and SnO₂/C confirms the nature of the conversion reaction with detectable end products, Sn and Na₂O (Fig. 9(e) and (f)). All observed diffraction rings belong to either Sn or Na₂O. The distribution of the Sn nanoparticles within the Na₂O matrix of the converted SnO₂/C electrode is uniform with an average Sn particle size around 2–5 nm (Fig. 9(b) and (d)). In contrast, the Sn nanoparticles that formed in the converted SnO electrode show random particle size distributions. The density of Sn within the Na₂O matrix was higher, as expected, due to the

higher Sn:O atomic ratio in SnO than in SnO₂. This difference results in a more clear and distinct diffraction rings of the SnO sample, while the SnO₂/C sample exhibits diffusive rings. The discrepancy in particle size of nano-Sn particles formed in SnO and SnO₂/C during the conversion step can be explained by the different morphologies of these samples: 1. the particle size of SnO₂/C is much smaller than that of SnO; 2. SnO₂ has been coated with a carbon layer during the hydrothermal reaction, which acts as a barrier against agglomeration.

After the first charge to 2.0 V, the particles grew in both electrodes as shown in Fig. 10. Although charging results in particles with reduced crystallinity, the SAED patterns (Fig. 10(e) and (f)) could be indexed to SnO₂ and Sn. After charging the converted SnO electrode up to 2 V, the Sn and Na₂O did not reverse back to the

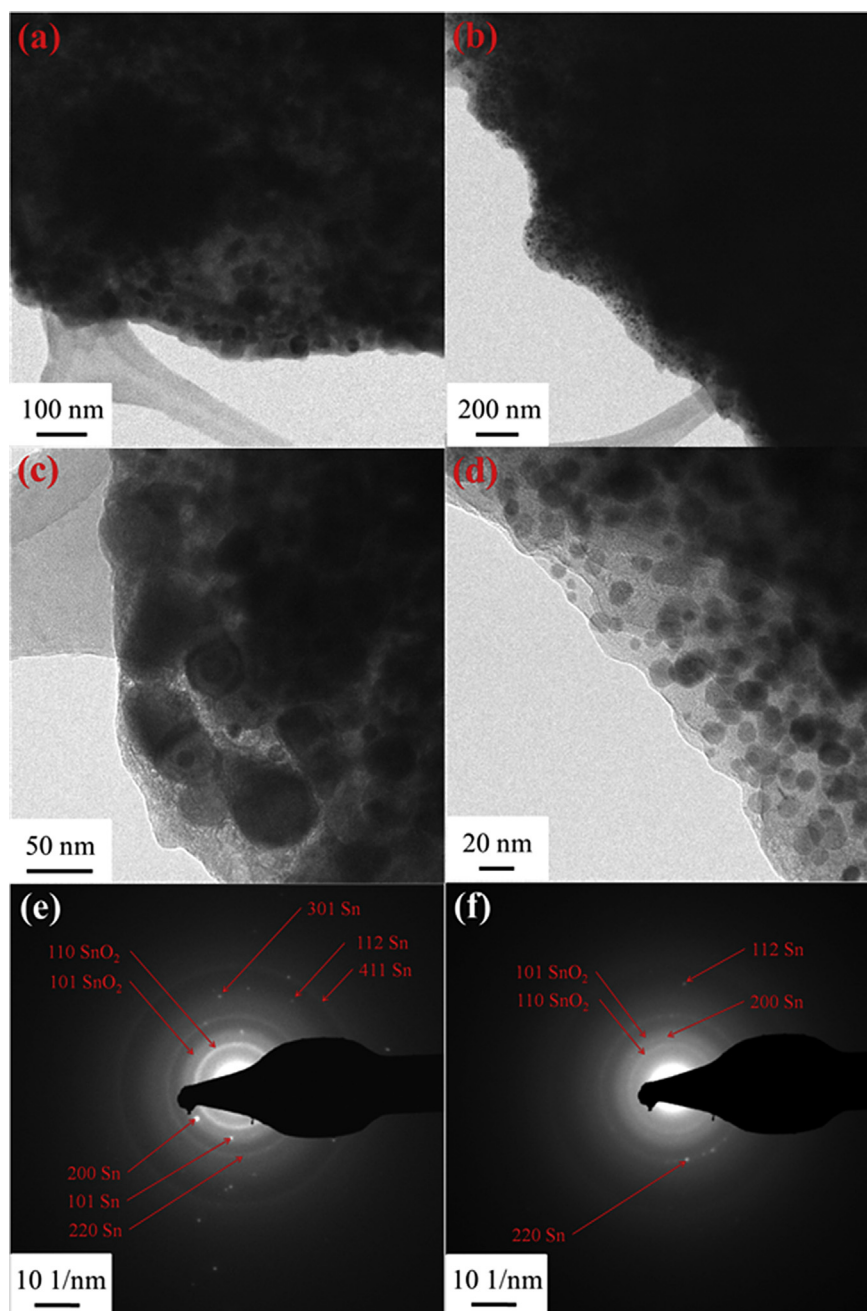
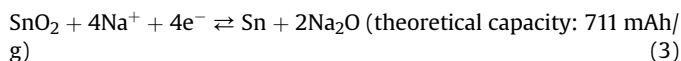
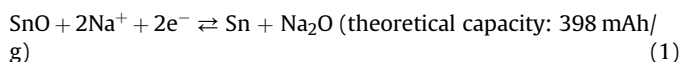


Fig. 10. TEM images: (a), (c) SnO; (b), (d) SnO₂/C after charged to 2 V; (e) SAED pattern of SnO charged to 2 V; (f) SAED pattern of SnO₂/C charged to 2 V.

pristine SnO because SnO₂ is the only thermodynamically stable phase. Notably, after charging to 2 V, the intensity of Sn reflections of the converted SnO electrode are much stronger than SnO₂/C (Fig. 8), which can be attributed to the higher Sn: O atomic ratio in SnO.

The results of the *ex-situ* XRD and TEM explain the rapid capacity fading of the SnO₂ and SnO₂/C samples. This is caused by the large volume expansion and low conductivity of the resulting electrode upon conversion, as discussed above. Based on conversion and alloying reaction, the discharge/charge reaction of SnO and SnO₂ can be expressed in the following:



The initial sodiation capacity of SnO₂ was 750 mAh/g (4.2 Na/mol) shown in Fig. 7(b). This indicates that the charge/discharge mechanism is 95% conversion reaction and 5% alloying reaction of Sn and Na.

In the case of SnO, the theoretical capacity of 2Na/mol conversion reaction of SnO is 398 mAh/g-SnO, the initial sodiation capacity of SnO was 720 mAh/g (3.6Na/mol) (Fig. 7(a)). This demonstrates that the charge/discharge mechanism is 55% conversion reaction and 45% alloying reaction of Sn and Na. In Fig. 6(a), SnO anode shows lower reversibility in conversion reaction region. However, the reversibility is recovered by having a lower voltage cutoff attributed to the reversible alloying reaction. Therefore, the remarkable difference in the cycling performance in Fig. 5 can be explained by the various degrees of the alloying reactions in the sodiation capacity.

In Fig. 11, the Nyquist plots of SnO and SnO₂/C electrodes at their pristine state and after the initial recharge (i.e. OCV → 5 mV → 2.0 V at 50 mA g⁻¹) are demonstrated. Clearly, SnO electrodes show a much lower charge transfer resistance in their pristine state (Fig. 11(a)) and after completion of the conversion cycle (Fig. 11(b)). Although SnO₂/C shows larger impedance than SnO/C at the initial state, it was reduced by the remained Sn after the first cycle. However, SnO/C exhibits a much higher reversible capacity and improved rate capability compared to both SnO₂ and SnO₂/C electrodes. Because the conductivity of the electrode is proportional to Sn content in the Na₂O/Sn. In addition, the carboxymethyl cellulose (CMC) binder used here plays an important role to keep the good electrochemical performance, because CMC have good electrolyte wettability [23] and could assist the formation of the good SEI layer [24] which allowed the Na ion diffusion easily.

Notably, the low polarization in SnO can be attributed to the lower oxygen content of SnO, giving rise to higher electrode conductivity.

4. Conclusions

Three anode materials: SnO, SnO₂, and SnO₂/C were prepared by hydrothermal reactions. Their potential applicability as anode materials for SIB were explored. A uniform SnO₂/C nanoparticle sample was obtained in the presence of glucose. SnO₂/C showed better capacity and capacity retention compared to bare SnO₂. Although SnO had larger particles, more uneven particle size, and particle distribution, it outperformed both SnO₂ and SnO₂/C. The

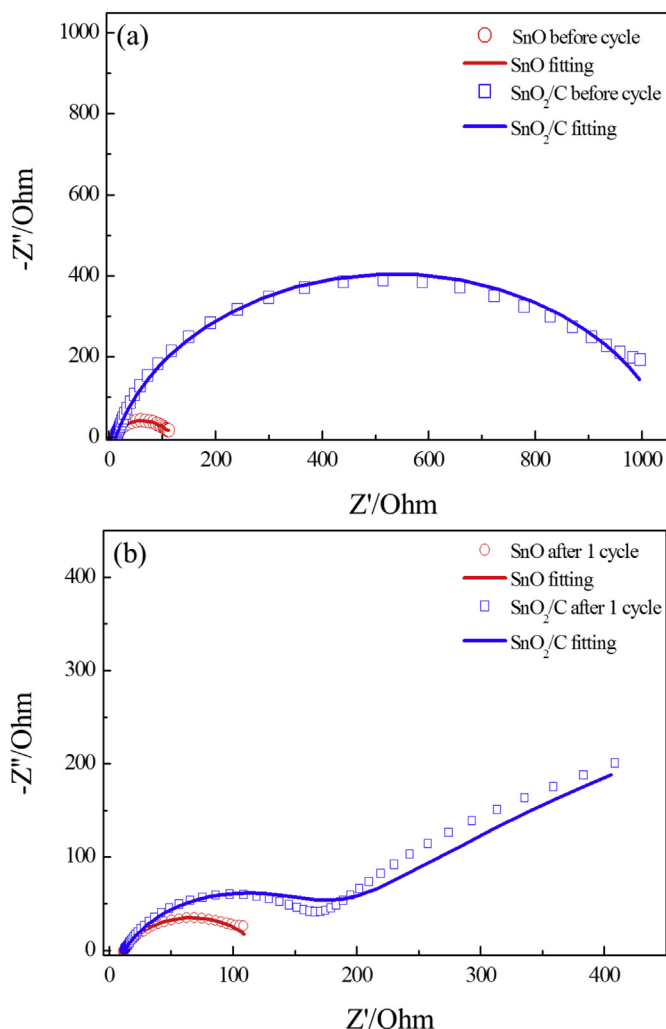


Fig. 11. Nyquist plots of SnO and SnO₂/C electrodes in their pristine state (a) and after the conversion cycle (b).

material demonstrated high reversible capacity, low polarization, and low irreversible capacity loss. SnO is the only sample in the studied series that did not show capacity loss over at least 50 cycles, and Sn utilization increased over cycles. This suggests that the Sn:O ratio and the respective Sn:Na₂O ratio in the converted electrode play an important roles. This also determine the electrochemical performances of the candidate anode materials. This work demonstrates the possibility of using SnO_x as a possible anode for both SIBs and LIBs. Further improvements are necessary to make such application feasible.

Acknowledgments

This work was financially supported by the Elements Science & Technology Projects of MEXT, Japan. C. Z. Ma, J. Alvarado and Y. S. Meng acknowledge the funding support by USA National Science Foundation under Award Number DMR1057170.

References

- [1] J.J. Braconnier, C. Delmas, C. Fouassier, P. Hagenmuller, *Mater. Res. Bull.* 15 (1980) 1797.
- [2] S. Okada, Y. Takahashi, T. Kiyabu, T. Doi, J.-I. Yamaki, T. Nishida, *Extended Abstracts of 210th ECS Meeting at Cancun, B2, #201, 2006.*
- [3] J. Zhao, J. Xu, D.H. Lee, N. Dimov, Y.S. Meng, S. Okada, *J. Power Sources* 264

- (2014) 235.
- [4] J. Xu, D.H. Lee, Y.S. Meng, *Funct. Mater. Lett.* 6 (2013) 1330001.
- [5] V.L. Chevrier, G. Ceder, *J. Electrochem. Soc.* 158 (2011) A1011.
- [6] B. Jache, P. Adelhelm, *Angew. Chem. Int. Ed.* 53 (2014) 10169.
- [7] S. Komaba, Y. Matsuura, T. Ishikawa, N. Yabuuchi, W. Murata, S. Kuze, *Electrochem. Commun.* 21 (2012) 65.
- [8] A. Darwiche, C. Marino, M.T. Sougrati, B. Fraisse, L. Stievano, L. Monconduit, *J. Am. Chem. Soc.* 134 (51) (2012) 20805.
- [9] J. Qian, Y. Chen, L. Wu, Y. Cao, X. Ai, H. Yang, *Chem. Commun.* 48 (2012) 7070.
- [10] L. Wu, X. Hu, J. Qian, F. Pei, F. Wu, R. Mao, X. Ai, H. Yang, Y. Cao, *Energy Environ. Sci.* 7 (2014) 323.
- [11] J. Qian, X. Wu, Y. Cao, X. Ai, H. Yang, *Angew. Chem. Int. Ed.* 52 (2013) 4633.
- [12] Y. Kim, Y. Park, A. Choi, N. Choi, J. Kim, J. Lee, J.H. Ryu, S.M. Oh, K.T. Lee, *Adv. Mater.* 25 (2013) 3045.
- [13] L. Xiao, Y. Cao, J. Xiao, W. Wang, L. Kovarik, Z. Niewa, J. Liu, *Chem. Commun.* 48 (2012) 3321.
- [14] M.K. Datta, R. Epur, P. Saha, K. Kadakia, S.K. Park, *J. Power Sources* 225 (2013) 316.
- [15] S. Komaba, W. Murata, T. Ishikawa, N. Yabuuchi, T. Ozeki, T. Nakayama, A. Ogata, K. Gotoh, K. Fujiwara, *Adv. Funct. Mater.* 21 (2011) 3859.
- [16] M. Shimizu, H. Usui, H. Sakaguchi, *J. Power Sources* 248 (2014) 378.
- [17] D. Su, X. Xie, G. Wang, *Chem. Eur. J.* 20 (2014) 3192.
- [18] D. Su, C. Wang, H. Ahn, G. Wang, *Phys. Chem. Chem. Phys.* 15 (2013) 12543.
- [19] Y. Wang, D. Su, C. Wang, G. Wang, *Electrochem. Commun.* 49 (2013) 3131.
- [20] D. Su, H.J. Ahn, G. Wang, *Chem. Commun.* 49 (2013) 3131.
- [21] F.I. Pires, E. Joanni, R. Savu, M.A. Zaghete, E. Longo, J.A. Varela, *Mater. Lett.* 62 (2008) 239.
- [22] M.A. Macías, J.A.H. Martínez, G.H. Gauthiera, J.E. Rodríguez, H. Avilab, J. Pintoa, J. Pinilla, *Mater. Res.* 14 (2) (2011) 172.
- [23] L. Gong, M.H.T. Nguyen, E.S. Oh, *Electrochem. Commun.* 29 (2013) 45.
- [24] J. Lia, R.B. Lewis, J.R. Dahn, *Electrochem. Solid State. Lett.* 10 (2007) A17.